THE ASTROPHYSICAL JOURNAL, 424:800–816, 1994 April 1

FLIERs AND OTHER MICROSTRUCTURES IN PLANETARY NEBULAE. II.[1]

BRUCE BALICK[2]
Astronomy Department, Univeristy of Washington; and Osservatorio di Arcetri, Firenze. email: balick@astro.washington.edu
M. PERINOTTO AND A. MACCIONI[3]
Departimento di Astronomia e Scienza dello Spazio, University of Firenze. email: mariop@arcetri.astro.it; maccioni@arcetri.astro.it
AND
YERVANT TERZIAN AND A. HAJIAN[4]
Astronomy Department and NAIC, Cornell Univeristy. email: terzian@astrosun.tn.cornell.edu; hajian@astrosun.tn.cornell.edu
Received 1993 July 29; accepted 1993 October 8

ABSTRACT

We report continued detailed spectroscopic studies of highly articulated structures, called "microstructures," in NGC 6543, 6826, and 7009. Of particular interest of these PNs are FLIERs (fast, low-ionization emission regions) characterized by the following:

ionization—much lower ionization than immediately adjacent gas;
size—small size in at least one dimension ($\approx 2''$, or about 0.01 pc at a distance of 1 kpc);
morphology—generally ansae, jets, knots, or strings of knots;
distribution—pairs (or sets of pairs) on equal and opposite sides of the central nucleus located near a nebular symmetry axis;
velocity—each partner has equal and opposite highly supersonic velocity ($\approx \pm 50$ km s^{-1});
kinematic age—the kinematic age (projected distance/redshift) of some FLIERs is less than that of the rest of the PN;
N abundance—apparent enhancement of nitrogen (only) relative to hydrogen by factors of 2–5;
kinetic/thermal energy density—much higher kinetic energy per mass than thermal energy; and
mass—typically 10^{-4} to 10^{-5} $M_\odot$,

and yet FLIERs exhibit little difference in density or temperature from their surroundings.

These properties and their small kinematic ages lead one to expect that FLIERs are high-density, opaque (i.e., partly neutral), and highly collimated material expelled recently from the nucleus. Their high ram pressure (10 times greater than the thermal pressure of the confining gas) should lead to the formation of bow shocks. Contrary to intuitive expectations, however, most FLIERs show the ionization structure expected of bow shocks. No simple model accounts naturally for the observed properties of FLIERs.

Subject headings: ISM: structure — planetary nebulae: general

1. INTRODUCTION

Most previous spectroscopic observations of planetary nebulae (PNs) have explored their global properties, such as chemcial abundances, excitations, temperatures, and densities. However, narrow-band images in the lines of marginal ionization states such as N^+ and O° have revealed a wealth of various small "microstructures." In many cases the properties of the microstructures deviate from the rest of the nebula. In this paper we explore selected microstructures spectroscopically.

Microstructures are characterized by arcsecond-like scale sizes, or $\approx 10^{16}$ cm at the characteristic distance of PNs of 1 kpc. The sound crossing time of microstructures is a few hundred years, short compared to the presumed nebular lifetimes (i.e. expansion lifetimes) of several thousand years. If microstructures are at higher pressure than their surroundings, as one might guess from their locally high emission measures seen in low-ionization lines, then their hydrodynamical lifetimes are far shorter than the nebular age. Alternately, they are maintained by external pressures from an unseen agent, such as the winds emitted by nearby PN nuclei. Numerous examples of microstructures in elliptical PNs are shown and identified in Figure 1.

The existence of small features of low ionization in PNs, often called "ansae" (handles), dates back to early work by Aller (1941). Aller and his colleagues, in papers far too numerous to be cited individually, have observationally pursued their characteristics for half a century. For the most part, these features were assumed to be the partially neutral regions through which stellar ionizing radiation does not penetrate. Of particular note are the results obtained for NGC 6543 and 7009 by Walker & Aller (1970) who showed that some microstructures had rather anomalous spectral properties for ionization fronts.

Reay & Atherton (1985) studied the kinematics of microstructures in NGC 7009 in the line of [O I]. They found that two, and perhaps four, of the low-ionization microstructures are moving supersonically with respect to the main body of the PN. Many other pairs of such features have been identified and studied by others. Balick, Preston, & Icke (1987, hereafter BPI) showed that the low-ionization features come in pairs along

[1] DEDICATION.—This paper is dedicated to Professor Lawrence Aller, a tireless researcher, an inspiring colleague, and the referee of this paper, on his 80th birthday.

[2] Postal address: Astronomy Department FM-20, University of Washington, Seattle WA 98195.
[3] Postal address: Osservatorio Arcetri, Largo Enrico Fermi 5, 50125 Firenze, Italy.
[4] Postal address: Astronomy Department, Cornell University, Ithaca, NY 14853.

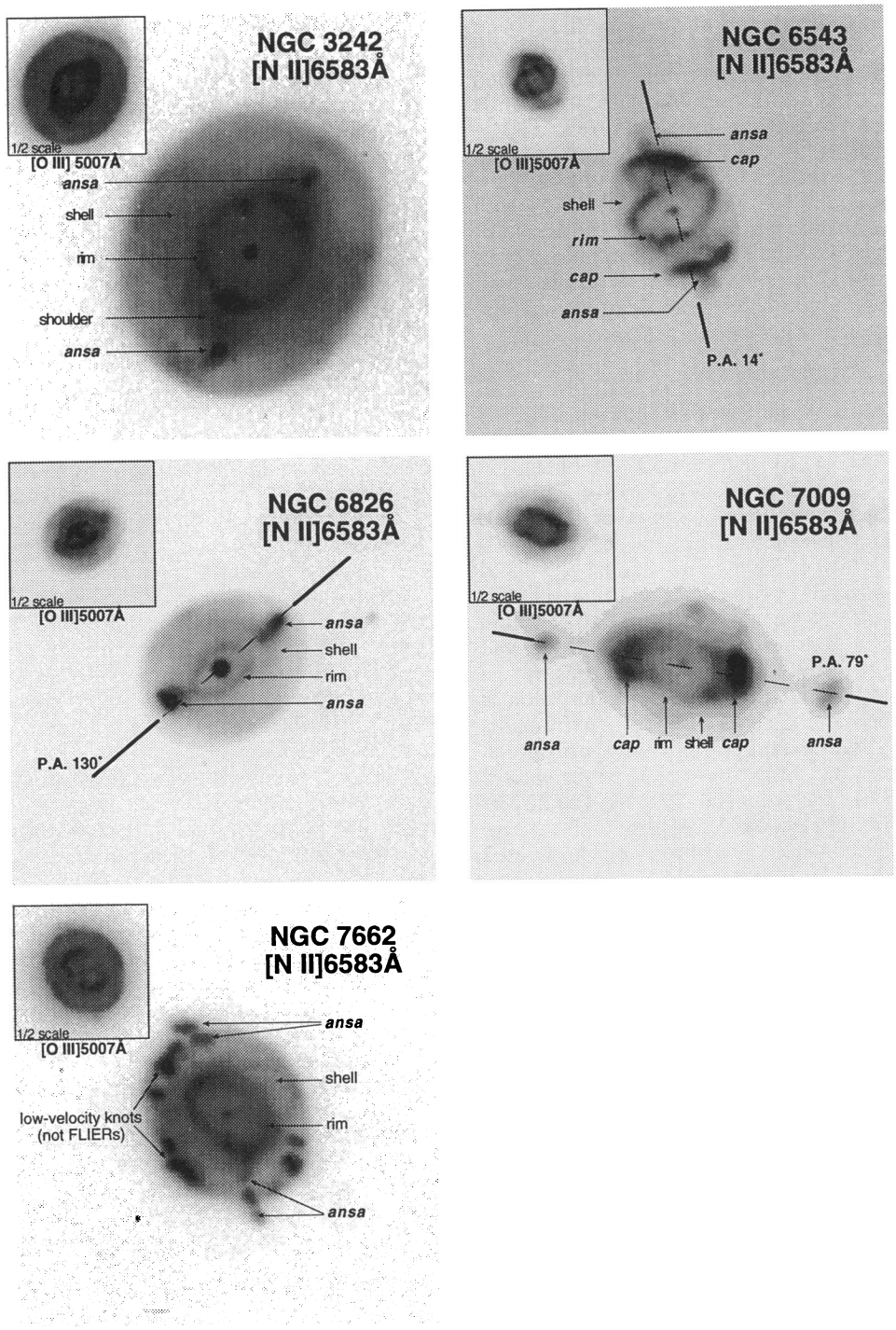

FIG. 1.—CCD images in the light of [N II] and [O III] (*insert*) of PNs of this paper and Paper I, taken from Balick (1987). N is at the top. The field of view of the [N II] image is 72″. Key morphological components ("features") are identified, and those that qualify as FLIERs are shown in bold italics. The location and the orientation of the 2′ long, 1″.5 wide slit is shown for those PNs discussed in the present paper (the projection of the slit on the nebula is not to scale).

the nebular symmetry axis, and that highly supersonic motions were commonly observed in [N II] lines from such features in elliptical PNs. They pointed out that the morphologies of the low-ionization features require a highly effective collimation process at the point of ejection or during the propagation of the gas but were unable to find a suitable mechanism. Observationally, some sort of strong hydrodynamic interaction, such as a shock, can be expected to be associated with such microstructures. Soker, Livio, and their colleagues have suggested that the most viable mechanism for generating collimated outflows along the nebular symmetry axis is likely to be ejection from mass-exchange binary systems.

Balick et al. (1993, hereafter Paper I) explored the spectroscopic properties of the microstructures in three PNs, NGC 3242, NGC 7662, and IC 2149. Their observations emphasized pairs of high-velocity (≥ 25 km s^{-1}) low-ionization knots and

radial "jets" on opposite sides of PN nuclei along the nebular symmetry axis which they called FLIERs (for fast-low-ionization emission regions). The symmetrical distribution of FLIERs and their relatively short kinematic ages suggest that FLIERs are knots ejected recently by the nucleus.

Here we extend the observations of Paper I to include NGC 6543 (G096.4+29.9 in the notation of Acker et al. 1992). NGC 6826 (G083.5+12.7), and NGC 7009 (G037.7−34.5) with observations of higher quality. Our focus here is on the physical and chemical properties of the FLIERs (identified in Fig. 1) and other small features of these PNs. The new results reveal important new information (though still no clear explanation) for the origin and evolution of these microstructures.

2. OBSERVATIONS

Hereafter, as in Paper I, we shall use the following abbreviations: [N II] = [N II] λ6583, [O I] = [O I] λ6300, [O II] = [O II] λ3727 = [O II] λλ(3726+3729), [O III] = [O III] λ4959, and [S II] = [S II] λλ(6717+6731). The subscripts "aur" and "neb" represent the sum of all optical auroral and nebular line intensities, respectively; e.g. $[O\ II]_{aur}$ = [O II] λλ(7319+7330) and $[S\ II]_{neb}$ = [S II] λλ(6717+6731). "Low- (high-)ionization" regions are characterized by the dominance of He° (He^{+} and/or He^{++}) within the PN's H II region. Ionization potential is I.P., and N = north, W = west, S = south, E = east, respectively.

The present observations were conducted using the Palomar 5 m (200 inch) telescope and double spectrograph on the nights of 1992 September 27–28. Standard gratings and spectrograph configurations were used to obtain two simultaneous spectra in the blue (3400–5150 Å) and red (5150–7600 Å). The dispersion is 2.1 Å $pixel^{-1}$ in the blue and 3.1 Å $pixel^{-1}$ in the red, and the effective resolution of the spectrograph is about 2 pixels, or close to 300 km s^{-1}. Along the slit each pixel is 0.″58 for the red camera and 0.″78 for the blue camera. Guiding was performed on the red images of bright stars in a nearby part of the sky.

The seeing averaged 1.″5 for the present observations. The weather was extremely variable on the first night, and the transparency changed from poor to excellent during exposures (typically 3–360 s) lasting more than a few minutes. For these reasons we endeavor to present only relative line intensities measured along the 1.″5 wide, 2′ long slit.

For each nebula the spectrograph slit was oriented to include a pair of FLIERs on opposite sides of the central star. The location of the slit is shown in the panels of Figure 1 showing NGC 6543, 6826, and 7009. Data were calibrated using standard IRAF procedures. The calibrated data and identified lines for one exposure on NGC 6543 are illustrated in Figure 2.

Atmospheric dispersion was not important for observations of the standard stars. However, the PNs were observed at a variety of airmasses and seeing conditions. In this case atmospheric dispersion can be a malicious problem. Obviously its effect on large features is not important. However, for small objects, especially those falling near the edge of the slit, signficant amounts of blue light can be lost. This explains the apparent blue turndown in the continuous spectrum of the PN nucleus in Figure 3. The only important lines likely to be affected are the [O II] λ3727 lines. For these lines the fluxes relative to Hβ are uncertain by about 10%, depending on the airmass, slit position angle, offset of the feature from the slit center, and the seeing at the time of observation.

Strong lines such as Hα and [O III] saturate the detector on the longer integrations (typically ≥10 s for NGC 6543 and 7009; ≥30 s for NGC 6826). Consequently the fluxes of strong and weak lines, or even Hα and Hβ, cannot be measured from a single exposure. The variable cloudiness of the first night means that the intensities of bright lines reported here have been scaled from the short exposures by using strong lines that were not saturated in any spectrum (often Hδ, He I λλ4471, 5876, and 7065). This procedure seems to have been successful except that the absolute fluxes of the lines are not known. The absence of absolute flux information is not of any consequence in this paper.

Long exposures were generally repeated 3 or 4 times so that nonrepeatable events, such as cosmic-ray hits, could be identified and removed from the data prior to averaging. Continuum emission was treated as part of the background and removed. "Slit brightness profiles" (one-dimensional plots of line emissivity as a function of slit position) and the spectra of specific features (such as FLIERs) were extracted. Representative spectra for important nebular features (defined in Fig. 1) were averaged over 2″–4″ and are plotted logarithmically in Figure 3. These spectra are from long integrations in which the bright lines are saturated.

Relative line intensities of emission lines were measured from these slit-averaged spectra both by integrating the flux under the lines or, more accurately, fitting multiple Gaussian profiles. The results of the Gaussian-fitted line intensities are shown in Tables 1–3. These are normalized to Hα (Hβ) = 100 for the red (blue) spectra.

We next discuss other problems which can affect the accuracy of the relative line intensities. For relatively bright lines, operationally defined to be those with more than about 500 electrons per pixel, we find from comparisons of repeated spectra that the relative line intensities repeat to better than 10%. By comparing the nubular continuum where the red and blue spectra join, we find that the calibration inconsistencies between the red and blue spectra are also about 10%. Consequently, since the two types of errors are independent, and ignoring the systematic errors caused by atmospheric dispersion (see above), we expect that line ratios of lines from different spectral regions are accurate to within 15%.

The accuracy of the Hα/Hβ ratio bears special note. The two lines are measured through independent channels in the spectrograph. One or both lines are often saturated except in the shortest exposures. Because the Hα line is saturated in all but the short exposures, the Hα/Hβ ratio is obtained from different exposures of possibly different atmospheric transparency. Consequently, the ratio is uncertain by 20%. We shall adopt values of this ratio from other references wherein the ratio is likely to have been measured with more accuracy than possible here.

The detector suffers from slight nonlinearities at very low light levels (less than about 200 detected electrons per pixel) caused by "sticky" electrons which are not completely removed from pixels in one read cycle. Sticky electrons are detected, but not always in the proper location on the CCD. In effect, faint features have small tails in the wavelength direction unless the pixel initially contained at least 200 electrons. The net result is that, for faint lines, measured fluxes may be in error by an additional 15%.

Some peculiar problems affect the line fluxes shown in Tables 1–3. For weaker lines, the uncertainty of the results is dominated by the subjective choice of the relatively bright continuum level. In addition, the choice of pixel ranges used to

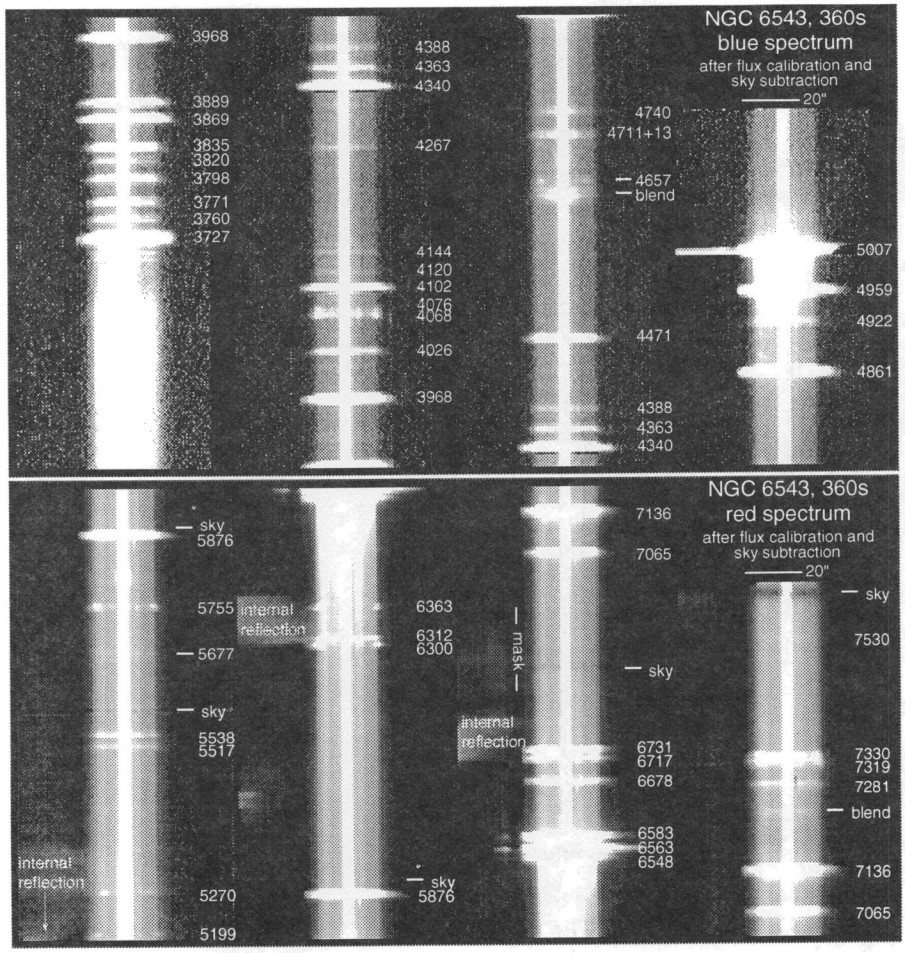

FIG. 2.—Representative data, in this case a 360 s exposure of NGC 6543. Both the red and blue spectra have been reformatted as four overlapping sections for display purposes. The data have been fully calibrated prior to display. Neither the stellar emission nor the nebular continuum have been subtracted. Only the lowest 1% of the intensities are shown in this very high contrast display. The wavelengths of the discernible lines are shown. Note the internal reflections on the left side of the spectra.

define the various features is somewhat arbitrary. This, and the steep brightness gradients of some lines across the range of pixels associated with sharp edges of many microstructures, mean that different definitions of the features sometimes yield relative line intensities that are uncertain by 10% (3 σ) and as much as 50% or more in rare cases.

Finally, no effort was made to subtract the spectra of extended emission regions from the spectra of microstructures. Thus the values of relative line intensities reported in Tables 1–3 represent integrals through the line of sight along which the fractional ionization of the elements or other physical conditions may vary.

3. QUALITATIVE RESULTS

Observational results which are obtainable by inspection of the data are summarized below.

3.1. *Line Identifications*

Identifications are based on tabulations of wavelengths and relative intensities by Aller & Keyes (1988), Solf, Böhm, & Raga (1988), Czyzak, Aller, & Kaler (1968), and other standard references.

As in Paper I, we identify a line at 4571 Å as Mg I]. This line, which was seen previously in other PNs (Paper I), is found exclusively in features where [O I] and other lines of very low ionization are relatively bright. Professor Aller suggests that a line near 5677 Å seen in NGC 6543 arises from N II.

At low brightness levels a series of faint, possibly confused lines appear in the spectra of NGC 6543 and 7009. Many of these lines fall at or very near the wavelengths of many forbidden lines of iron in various ionization stages. Their identification as lines of [Fe II] λ7154 and [Fe III] $\lambda\lambda$4657 + 5270 in the spectrum of NGC 6543 and [Fe V] λ4228 in NGC 7009 looks straightforward and without suitable alternative. Such identifications are made with some trepidation, however. For example, other expected lines do not appear (e.g. [Fe II] λ7452 in NGC 6543). Without deeper observations of higher dispersion, the identification of these faint lines as various Fe lines remains merely "plausible."

3.2. *Spatial Emission Distribution*

The slit brightness profiles of Hα, [N II], and [O I] are presented in Figure 4. Care was taken to extract all slit brightness profiles from a single unsaturated exposure with the highest possible signal-to-noise-ratios. A flat background was subtracted, and the line profile was integrated in the wavelength direction in order to produce a profile along the slit. Data near pixel 60, the nominal location of the central star, are unreliable

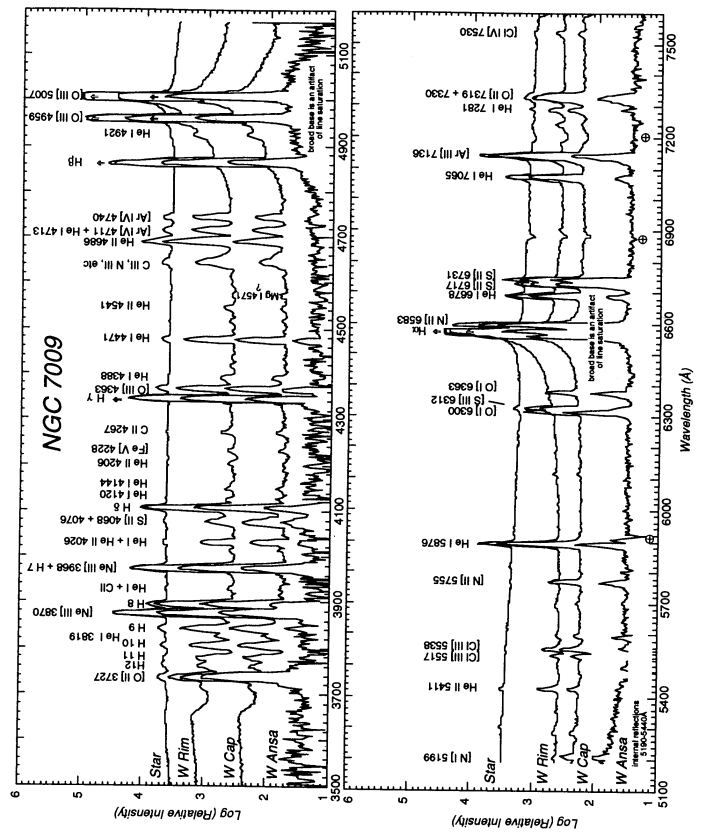

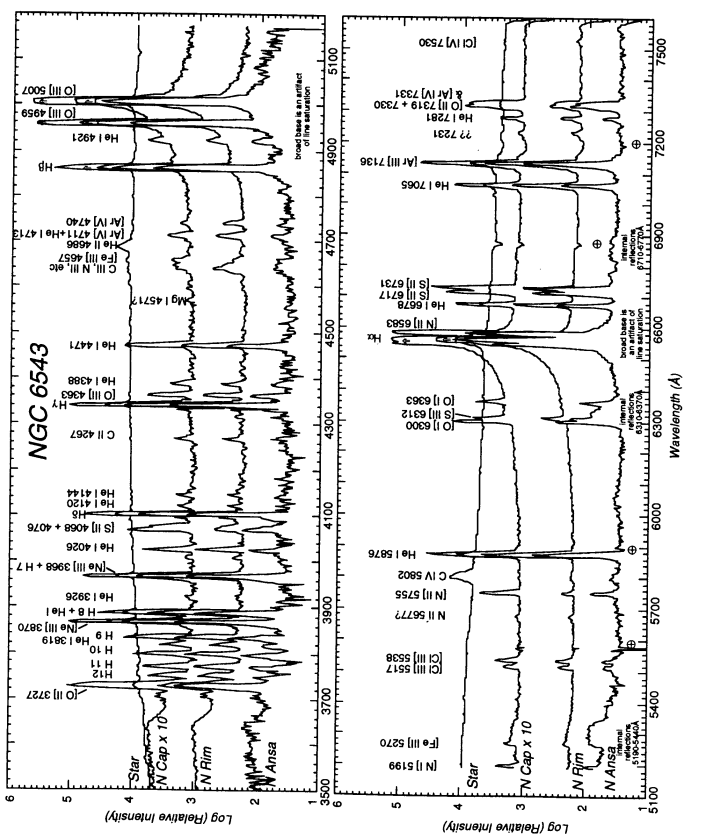

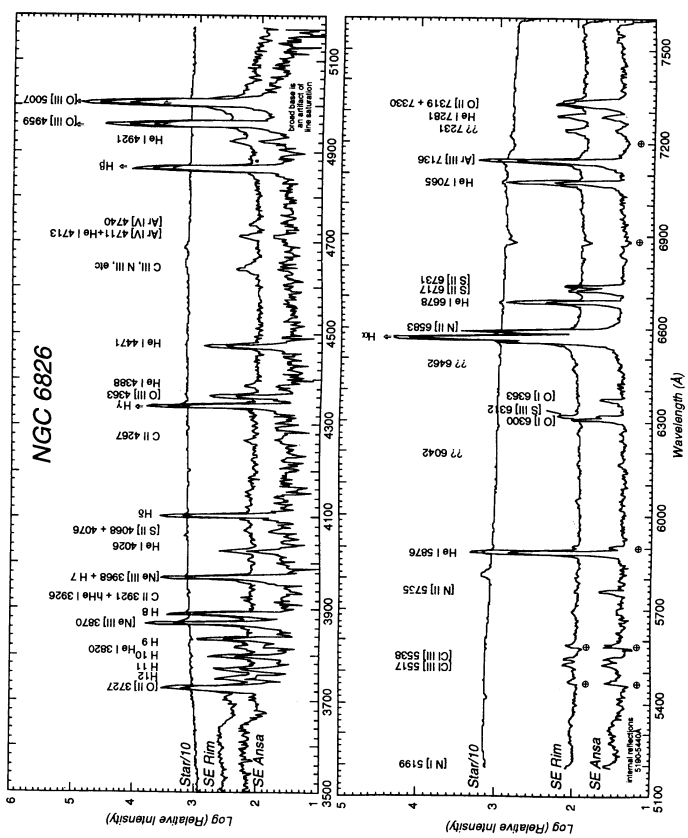

FIG. 3.—Spectra of selected morphological comonents ("features") of NGC 6543, NGC 6826, and NGC 7009, displayed as the logarithm of the intensity. These spectra are formed by averaging the brightest columns in a 360 s exposure CCD spectrum. The name of the feature and the integration time of its spectrum are indicated. Question marks indicate line with uncertain identifications. Regions affected by internal reflections or saturation are indicated along the bottom. Note the qualitiative changes in the relative strengths of low-ionization emission lines among the spectra.

owing to masking of the star or saturation of the detector. In addition, small residual alignment errors remain which can affect the measured line ratios, especially where intensity gradients are steep.

Strong ionization stratification along the slit is seen very clearly in all PNs observed (Fig. 4). Please note that the [O I] lines peak at larger radii from the nucleus than the [N II] lines. Also note that the Hα profile shows little if any sign of an intensity maximum at the position of the FLIERs. These same patterns, which are common characteristics of FLIERs, were also found in NGC 3242 and 7662. Observed at high dispersion ($\lesssim 10$ km s^{-1}), the ratio of [N II] to Hα at the location and redshift centroid of the FLIERs approaches unity in NGC 3242 and 7662 (Paper I and BPI). The simplest interpretation of the results is that FLIERs do not contribute significantly to the Hα flux, either because their H^+ abundance is low because their sizes are very small (or both). Further elaboration is presented in § 5.

Some other slit brightness profiles and their ratios are presented in Figures 5–7 following the same procedures used for Figure 4. In general, lines of moderate ionization (e.g., recombination lines of H^+ and He^+ as well as forbidden lines of O^{++}

TABLE 1

NGC 6543: SPECTRA OF SELECTED REGIONS

Line Identification	λ(Å)	N Rim	N Cap	N Ansae
Blue Spectra Relative to Hβ = 100				
[O II]	3727	17.6	51.8	37.8
H 12	3750	2.42	1.94	1.17
H 11	3771	2.92	2.05	1.56
H 10	3797	3.86	3.04	2.26
He I	3819	1.14	1.07	0.98
H 9	3835	5.93	4.68	3.59
[Ne III]	3869	44.4	36.2	27.1
H 8 + He I	3889	16.5	11.4	12.1
C II + He I	3921+3926	0.39	0.19	-.-
[Ne III] + H ε	3967	27.9	23.1	19.0
He I	4009	0.20	0.097	---
He I	4026	2.35	1.91	1.27
[S II] + C III:	4068+70	0.81	3.02	1.4:
[S II]	4076	0.51	1.54	0.6:
H δ	4102	23.1	18.5	16.4
He I:	4121	0.35	0.30	---
He I	4144	0.32	0.33	0.26:
C II	4267	0.62	0.40	0.28:
H γ	4340	42.1	37.2	35.4
[O III]	4363	1.86	1.76	1.80
He I	4388	0.67	0.61	0.74:
:line	4413	0.16	0.059:	---
:line	4432	0.15	---	---
He I	4471	5.50	5.05	4.76
Mg I:	4571	---	0.13	---
CNO III blend	4633-50	2.75:	1.64	1.25:
[Fe III]:	4657	0.68	0.85	0.97
[Fe III]:	4701	---	0.14	---
[Ar IV] + He I	4711+13	1.34	0.89	0.84
[Ar IV]	4740	0.88	0.32	0.39:
H β	4861	100	100	100
[Fe III]:	4881	---	0.24	---
He I	4921	1.48	1.42	1.75
[O III]	4959	243.	238.	216.
[Fe II or VII]:	5158	---	0.10:	---
Red Spectra Relative to Hα = 100				
[N I]	5200	-.-	0.19	0.31:
[Fe III]:	5270	0.11:	0.11:	-.-
[Cl III]	5518	0.16	0.18	0.13:
[Cl III]	5538	0.22	0.26	0.11:
N II:	5677	0.065	0.047	---
[Fe VII]:	5713	---	0.013:	---
[N II]	5755	0.12	0.62	0.40:
C IV:	5803	0.053	0.016:	0.15
He I	5876	5.84	5.18	4.99
[O I]	6300	0.065	1.60	1.59
[S III]	6312	0.40	0.64	0.8:
[O I]	6363	0.044	0.53	0.56
H α	6563	100	100	100
[N II]	6583	8.50	47.7	59.7
He I	6678	1.78	1.66	1.74
[S II]	6717	0.42	2.34	4.68
[S II]	6731	0.74	4.23	7.04
He I	7065	2.35	2.14	1.67
[Ar III]	7136	7.22	7.96	8.07
[Fe II]:	7154	0.039	0.066	0.099
:line	7231	0.13	0.063:	-.-
He I	7281	0.26	0.22	0.21
[O II]*	7319	0.57	1.61	1.64
[O II]*	7330	0.23	0.91	0.62
[Fe II]	7452	---	---	---
[Cl IV] + blend	7525-30	0.051	0.014:	---

* Contamination by [Ca II] λ7324 or [Ar IV] λ7331 is possible.

† Unknown or uncertain identification or poorly measured intensity.

TABLE 2

NGC 6826: SPECTRA OF SELECTED REGIONS

Line Identification	λ(Å)	SE Rim	SE Ansae
Blue Spectra Relative to Hβ = 100			
[O II]	3727	15.9	65.6
H 12	3750	2.44	1.93
H 11	3771	2.58	2.45
H 10	3797	3.37	3.00
He I	3819	0.75	1.40:
H 9	3835	5.24	4.56
[Ne III]	3869	39.1	30.2
H 8 + He I	3889	17.0	14.4
C II + He I	3921+26	0.49	-.-
[Ne III] + H ε	3967	26.5	21.4
He I	4026	2.01	1.68
[S II] + C III:	4068-76	0.41	0.77:
H δ	4102	23.0	19.5
He I	4121	0.22	-.-
He I	4144	0.17	-.-
CII + OII	4267+76	0.60	0.54:
H γ	4340	42.3	38.3
[O III]	4363	3.70	2.95
He I	4388	0.71	0.38:
He I	4471	4.75	4.43
C,N,O III blend	4633-50	2.00	-.-
[Ar IV] + He I	4711+13	1.04	4.0:
[Ar IV]	4740	0.45	0.22:
H β	4861	100	100
He I	4921	1.39	0.97
[O III]	4959	263.	222.
Red Spectra Relative to Hα = 100			
[N I]	5200	0.14:	0.10:
[Cl III]	5518	0.11	0.16
[Cl III]	5538	0.084	0.11
:blend	5690	0.074	0.067:
[N II]	5755	0.020	0.21
He I	5876	4.60	4.74
:blend	6042	0.03	-.-
[O I]	6300	-.-	0.62
[S III]	6312	0.17	0.22
[O I]	6363	-.-	0.17
:line	6462	0.043	0.020:
H α	6563	100	100
[N II]	6583	2.64	28.7
He I	6678	1.38	1.41
[S II]	6717	0.11	0.60
[S II]	6731	0.12	0.71
He I	7065	1.47	1.33
[Ar III]	7136	3.89	4.54
:line	7231	0.25	0.14
He I	7281	0.28	0.28
[O II]*	7319	0.35	1.50
[O II]*	7330	0.13	0.58

* Contamination by [Ca II] λ7324 or [Ar IV] λ7331 is possible.

† Unknown or uncertain identification or poorly measured intensity.

TABLE 3

NGC 7009: SPECTRA OF SELECTED REGIONS

Line Identification	λ(Å)	W Rim	W Cap	W Ansae
Blue Spectra Relative to Hβ = 100				
[O II]	3727	9.16	44.7	39.
H 12	3750	2.6:	2.5	-.-
H 11	3771	2.81	3.1	-.-
H 10	3797	3.20	4.2	-.-
He I	3819	0.84	1.1	-.-
H 9	3835	4.63	6.3	3.6:
[Ne III]	3869	68.2	93.8	132.
H 8 + He I + [Fe V]	3889	13.5	17.8	16.
CII + HeI	3921+26	0.19	0.23	-.-
[Ne III] + H ε	3967	33.6	43.0	59.
He I	4009	0.12	0.17:	-.-
He I + He II	4026	1.8	2.12	3.5:
[S II], C III, [Fe V]:	4068-76	1.9	4.30	11.0
H δ	4102	21.0	22.9	19.4
He I:	4121	0.33	0.28	-.-
He I	4144	0.36	0.34	-.-
He II	4206	0.30	0.14:	-.-
[Fe V]	4228	0.39	0.23	-.-
CII + OII	4267+76	0.56	0.48	-.-
H γ	4340	38.9	42.4	44.
[O III]	4363	6.04	7.1	10.
He I	4388	0.68	0.49	-.-
O II	4416	0.12:	0.05:	-.-
:line	4432	0.093:	0.06:	-.-
:line	4450	0.056:	-.-	-.-
He I	4471	4.51	5.06	4.4:
O II	4490	0.069:	0.11:	-.-
CNO III blend	4512	0.18	0.13:	-.-
He II	4541	0.46	0.21	-.-
Mg I:	4571	0.092	0.22:	-.-
:blend	4606	0.26	0.09:	-.-
CNO III blend	4633-50	0.46	2.95	-.-
He II	4686	13.2	5.88	-.-
[Ar IV] + He I	4711+13	3.42	2.53	0.7:
[Ar IV]	4740	3.29	2.06	2:
H β	4861	100	100	100
He I	4921	1.10	1.15	-.-
[O III]	4959	408.	439.	384.
Red Spectra Relative to Hα = 100				
[Ar III]	5191	0.015	-.-	-.-
[N I]	5200	-.-	0.20	1.14
[Fe III]:	5270	0.054	0.098	-.-
:line	5284	0.029	0.031:	-.-
He II	5411	0.28	0.13	-.-
[Cl III]	5518	0.10:	0.11:	-.-
[Cl III]	5538	0.23:	0.32:	-.-
[Fe VI]: + blend	5684	0.10	0.080:	-.-
:blend	5705	0.096	-.-	-.-
[N II]	5755	0.075	0.49	1.76
He I	5876	4.55	4.89	4.95
[Ca V] + [Fe VII]:	6080	0.018:	-.-	-.-
[K IV]:	6102	0.044	0.029	-.-
He II: + blend	6166-70	0.027:	0.034:	-.-
He II:	6234	0.008:	0.017:	-.-
[O I]	6300	0.067	1.61	8:
[S III]	6312	0.54	0.77	1:
Si II	6340	0.022:	0.012:	-.-
[O I] + Si II	6363+71	0.032	0.56	3:
H α	6563	100	100	100
[N II]	6583	4.23	31.3	123.
He I	6678	1.4	1.47	1.6
[S II]	6717	0.42	2.57	13.7
[S II]	6731	0.75	4.40	16.4
[K IV]:	6797	0.006:	0.019:	-.-
He I	7065	1.90	1.82	1.0:
[Ar III]	7136	5.88	7.80	9.8
:line	7231	0.11	0.054:	-.-
He I	7281	0.22	0.23	0.2:
[O II]*	7319	0.50	1.48	0.5:
[O II]*	7330	0.35	1.07	4:
[Cl IV] + blend	7525-30	0.12	0.085:	-.-

* Contamination by [Ca II] λ7324 or [Ar IV] λ7331 is possible.

† Unknown or uncertain identification or poorly measured intensity.

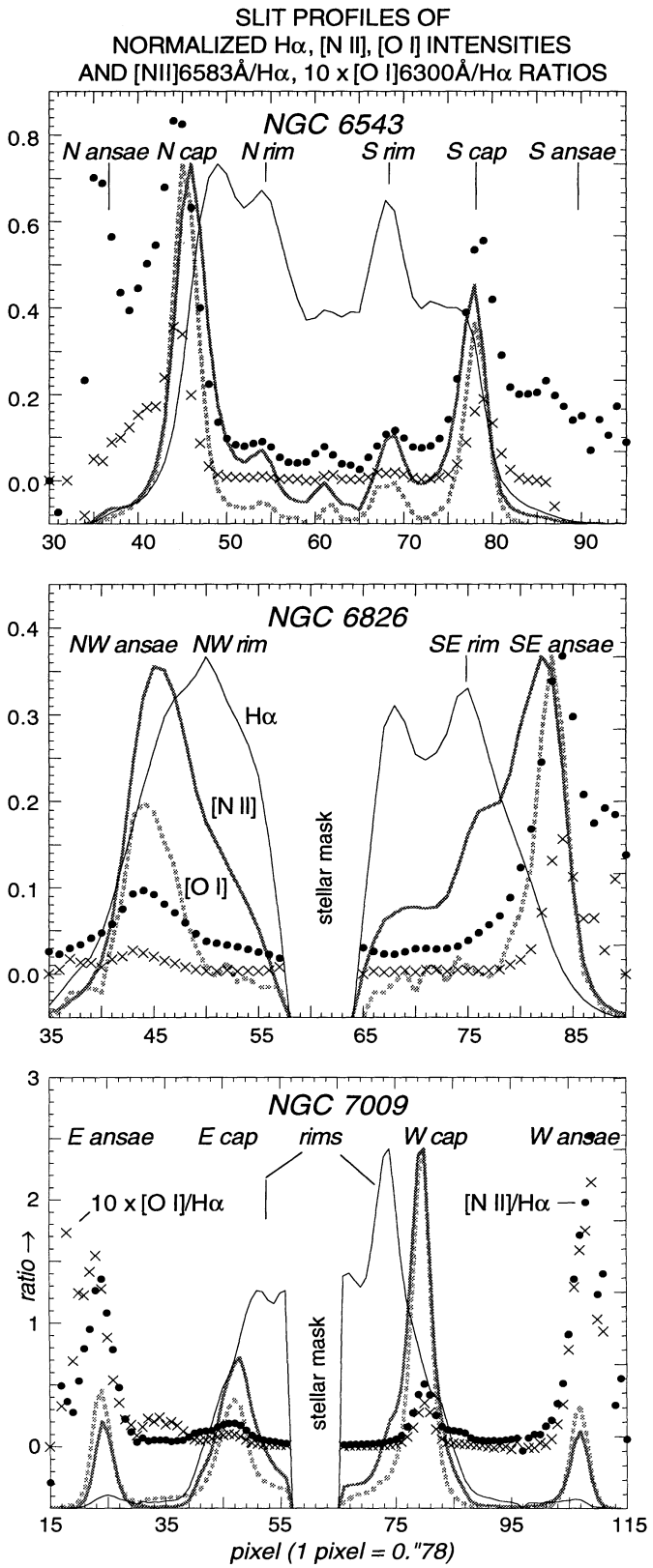

FIG. 4.—Slit intensity profiles in selected emission lines. Morphological features are defined in Fig. 1. The ratio scale on the left-hand side of the figure refers to the filled circles ([N II] 6583/Hα) and crosses (10 × [O I] 6300/Hα). Hα, [N II], and [O I] profiles have all been normalized to their peak intensities. The ratios shown in this figure are less averaged (i.e., have higher spatial and spectral resolution, with attendant lower signal-to-noise ratios) than those presented in Figs. 3–5 and Tables 1–3.

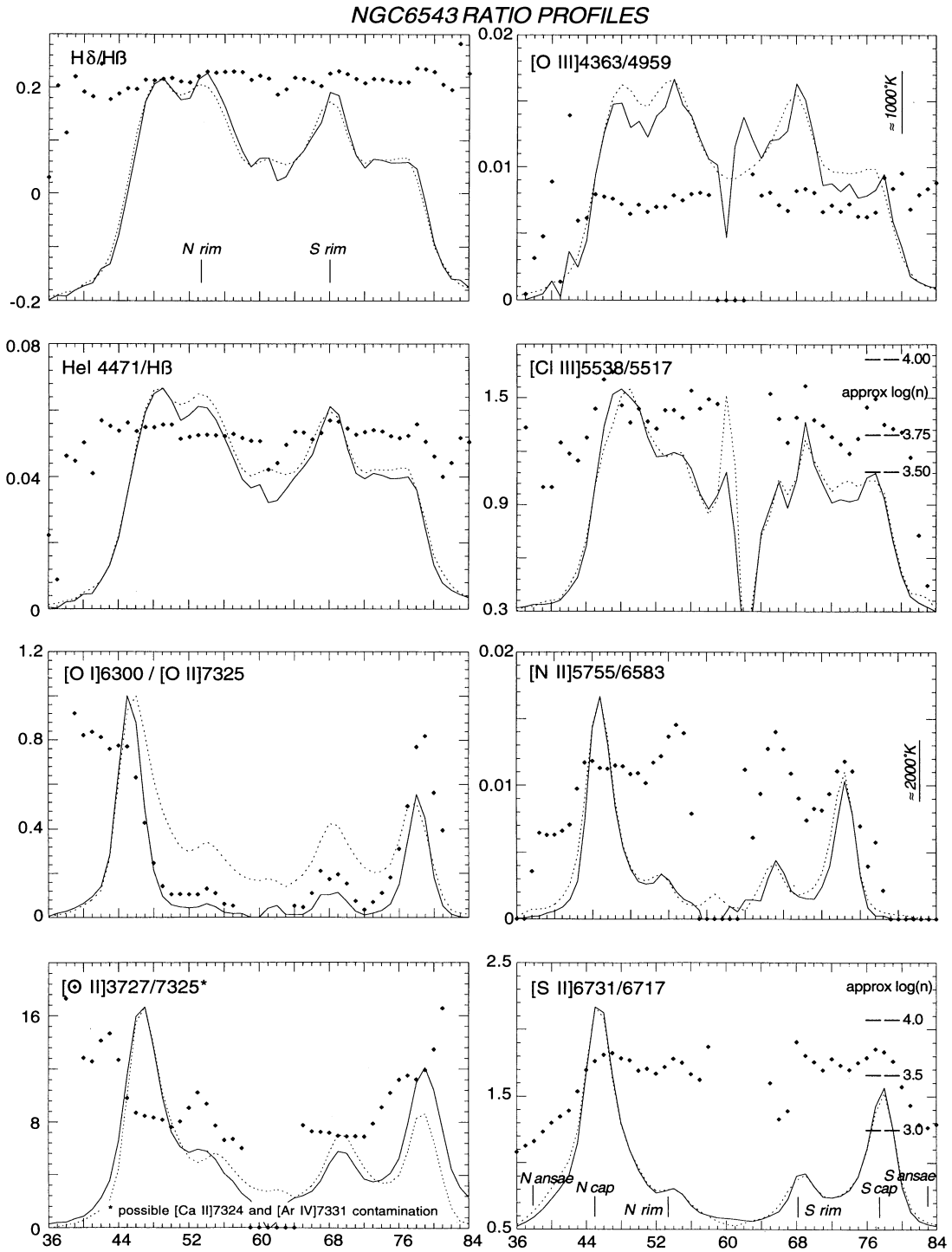

FIG. 5.—Additional slit intensity profiles and their ratios for NGC 6543. The profiles have been normalized to their peak for display purposes. The solid (dashed) line represents the intensity distribution of the numerator (denominator). Each pixel corresponds to 0".78. Points near pixel 60 are likely to be affected by starlight or a mask used to block the star. Ratios of the lines are shown as points, and the absolute scale of the ratios is shown on the left axis. Ranges of temperatures and densities are indicated on the right sides of the appropriate figures. Scales on the right sides of the panels are in arbitrary units.

and Ne^{++}) have nearly the same brightness distributions. This is expected if these lines arise from dominant ionziation stages, and if the electron temperature in the moderately ionized gas is fairly uniform. (Note that He^{++} is seen only in NGC 7009. Its extent is limited to that of the rims.) All lines from species of low ionization, such as N^+, O^+, S^+, N°, and O°, are generally similar in distribution along the slit to one another, but considerably different from the lines of higher ionization. [Ar III], [S III], and [Cl III] lines are intermediate in distribution between lines of moderate and low ionization, as expected. This ionization morphology also characterizes NGC 3242 and 7662.

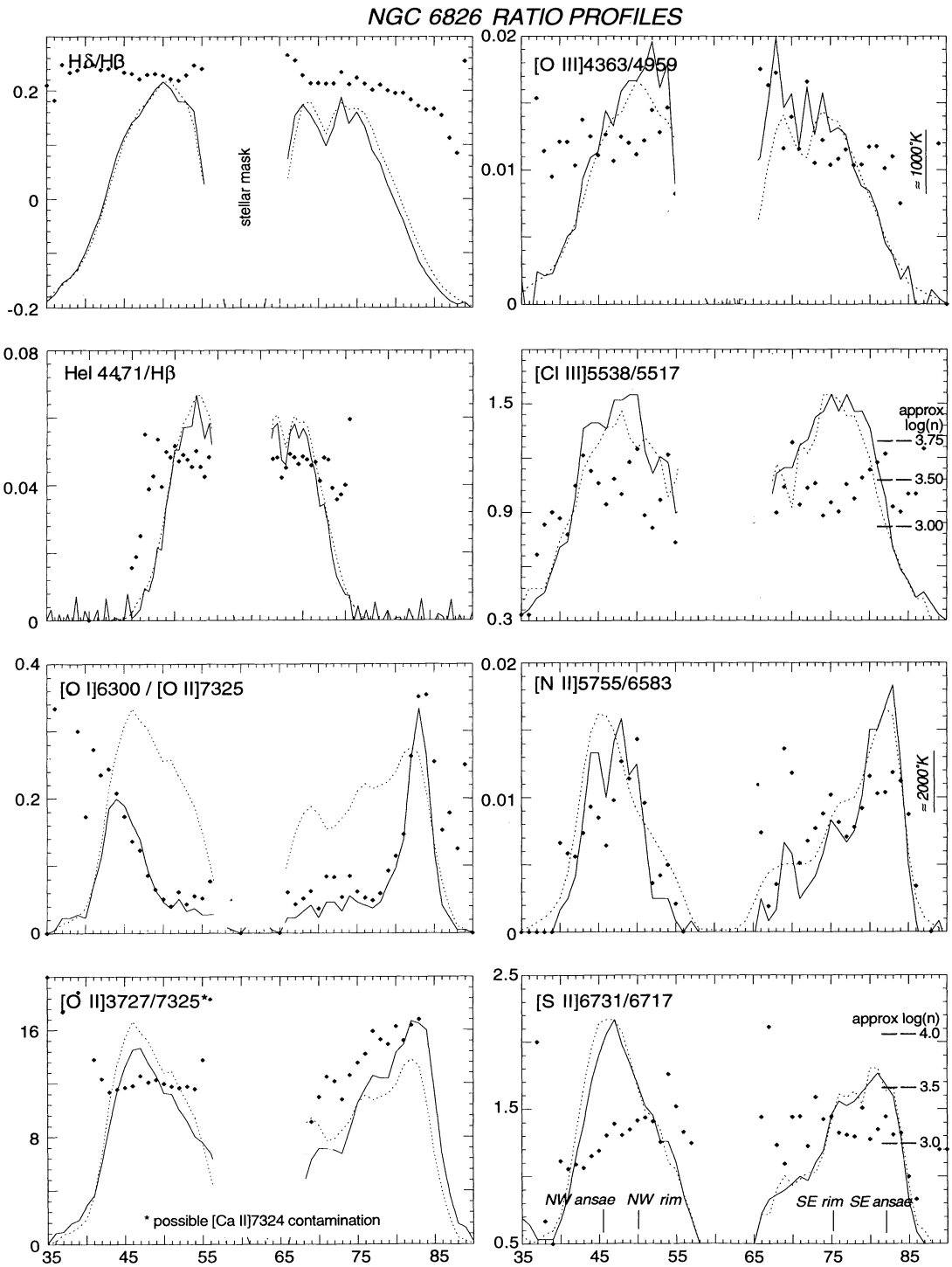

FIG. 6.—Like Fig. 7 except for NGC 6826

3.3. *Variations of Physical Conditions*

The discussion in this section is based on line ratio variations as shown in Figures 5–7 in which the locations of important features are indicated in the lower right panel. Owing to the crude method of removing background, ratios shown in the figures should be regarded as showing trends rather than optimum absolute values. (A detailed quantitative analysis follows in § 4 in which line fluxes are obtained by careful line fitting.)

3.4. *Extinction Variations*

These are indicated by changes in the Hδ/Hβ line ratio along the slit. No credible variations are seen in this ratio. However, since the FLIERs are very weak in the permitted lines, we

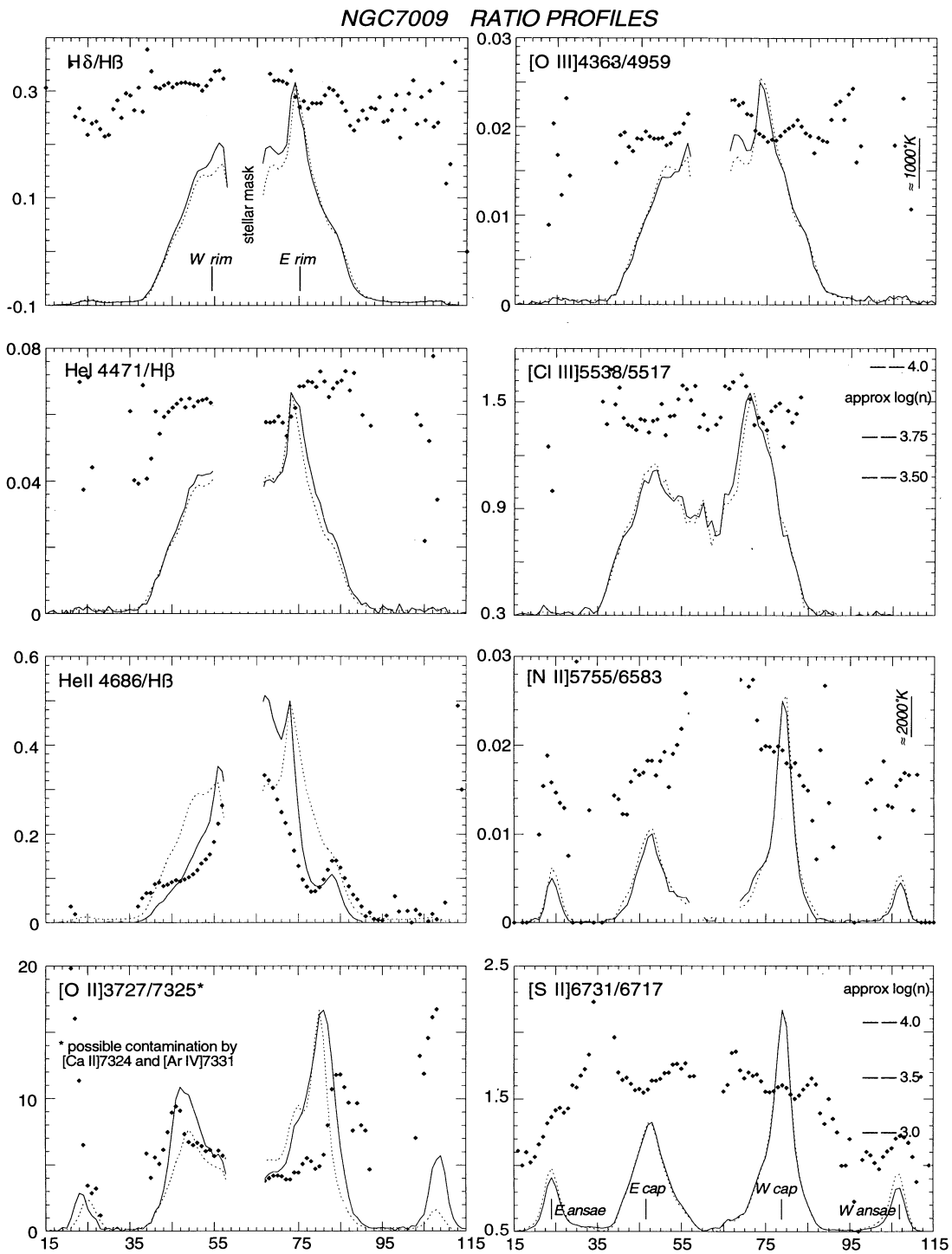

FIG. 7.—Like Fig. 7 except for NGC 7009

cannot isolate or independently estimate their internal extinctions. It will be interesting to determine reddening intrinsic to FLIERs using pairs of lines from the ^2P to the ^2D and ^4S levels in [S II] or [O II]. Note that Barker (1988, hereafter Ba88) finds that extinction increases in the direction of the NW FLIER of NGC 6826. Figure 6 shows no such change.

3.5. *Global Ionization and* He *Abundance*

Trends in He/H abundances with slit position are shown in Figures 5–7. As measured by the He I λ4471/Hβ ratio profile, there are no obvious variations in the He^+/H^+ ratio along the respective slits of NGC 6543 and 6826. Clearly NGC 7009 has

a small, ionization-bounded He^{++} zone trapped within the rims. However, the total He/H abundance, $(He^{+} + He^{++})/H^{+}$, appears to be constant. Absolute He abundances are derived in § 4.

3.6. *Density*

Densities n in the low-ionization and high-ionization zones are characterized by $n(S^{+})$ and $n(Cl^{++})$ which are derived from ratios of $[S\ II]_{neb}$ and $[Cl\ III]_{neb}$ lines, respectively. Densities are $\geq 10^3$ cm^{-3} and show little variation long the slit through the bright inner regions, as seen in Figures 5–7. At larger radii the densities generally seem to decline smoothly. [Obviously, the densities of FLIERs are best measured by $n(S^{+})$ since their [Cl III] lines are very weak.)

The important point here is that many FLIERs do not appear as separate, very dense knots or clumps of gas, perhaps a rather curious result. For sizes of $\approx 10^{-2}$ pc, their characteristic masses are 10^{-5} to $10^{-4}\ M_{\odot}$. Overall, similar results were found for the FLIERs discussed in Paper I.

3.7. *Temperature*

Temperatures in the low-ionization and high-ionization regions are measured by the [N II] and [O III] lines, $T(N^{+})$ and $T(O^{++})$, respectively, using expressions given by Osterbrock (1989). Figures 5–7 again indicate little variation in either $T(N^{+})$ and $T(O^{++})$ anywhere along the slit except, perhaps, at the outer edges of PNs where the auroral lines become noisy.

3.8. *Miscellaneous*

Another potentially interesting diagnostic line ratio is $[O\ II]_{neb}/[O\ II]_{aur}$. This ratio, shown in the lower left panels of Figures 5–7, is sensitive to both density and temperature (Aller 1984, Fig. 5.10). The red $[O\ II]_{aur}$ lines may be slightly contaminated by [Ca II] and/or [Ar IV] lines, and the blue $[O\ II]_{neb}$ affected by atmospheric dispersion problems as noted in § 2. In view of the inherent problems in the calibration process for lines at opposite ends of our red and blue spectra, the values of the $[O\ II]_{neb}/[O\ II]_{aur}$ appear to be consistent with the other, more accurate line ratio measurments of n and T already discussed.

Similarly, the $[S\ II]_{neb}/[S\ II]_{tr\ aur}$ ratio can potentially provide some useful constraints on the estimates of n and T where "tr aur" stands for transauroral. However, contamination of the $[S\ II]_{tr\ aur}$ lines by C III or other lines renders this ratio of little real use. We ignore it hereafter.

3.9. *Looking Ahead*

The observations seem to suggest that the FLIERs have about the same densities and temperatures as their immediate surroundings. An important issue in the context of subsequent discussions is whether this is actually true: perhaps the low ionization of FLIERs is simply the result of extremely high densities at which the rate of recombinations in, say, O^{++}, N^{++}, and S^{++} (which scales with ionic charge Z roughly as Zn^2, ignoring charge exchange and temperature variations) exceeds the reionization rate (which varies as n) in spite of the observational evidence. We ask: under what conditions can the densities be seemingly far in excess of those measured from the ratios of $[S\ II]_{neb}$ and $[Cl\ III]_{neb}$ lines?

The short answer to the question is "none," at least not for the objects studied here. Suppose that the low-ionization features were actually of such high density that their $[S\ II]_{neb}$ and $[Cl\ III]_{neb}$ lines were almost completely collisionally quenched. In this case, the observed nebular lines would arise in foreground/background gas and would not show any appreciable changes along the slit near the low-ionization features, as observed. However, the presence of the extremely dense regions could still be found in two ways, both exploiting the much higher critical density for collisional deexcitation, n_{crit}, of auroral and transauroral lines.

One method involves the emission of $[O\ II]_{aur}$ lines near 7325 Å. These should be emitting efficiently to densities of 10^6–10^7 cm^{-3} even if their nebular counterparts are largely quenched. However, our observations fail to show signs of unusually strong $[O\ II]_{aur}$ lines. The second method relies on auroral lines of [N II] and [O I] ($n_{crit} \approx 10^8$ cm^{-3}) which would tend to be much brighter relative to their corresponding nebular lines ($n_{crit} \approx 10^5$–10^6 cm^{-3}) in FLIERs than nearby. If the densities lie between 10^5 and 10^8 cm^{-3}, then relative to the nebular lines, the auroral lines of [N II] and [O I] would be brighter than in regions outside. In effect, an apparent temperature increase in FLIERs would be found, contrary to observations.

In summary, FLIERs appear to be distinguished from their surroundings primarily by their low ionizations and higher velocities. On the other hand, the FLIERs embedded within bright shells exhibit much the same values of n and T as their surroundings. Their ram pressure $P_k = \rho v^2/2$ exceeds their thermal pressure $P_{th} = 3kT/2$ by an order of magnitude, so strong hydrodynamic interactions and, perhaps surface turbulence are expected. In particular, shocks should exist since FLIERs are moving highly supersonically through a medium of comparable density and temperature. Can shocks explain the measured line ratios and their distributions along the slit? This is explored further in §§ 5 and 6.

4. PHYSICAL AND CHEMICAL CONDITIONS

The results in this section are based on the data of Tables 1–3, for which lines and the underlying adjacent continuum has been carefully fitted with Gaussian profiles, and overlapping lines have been deblended by fitting Gaussians of equal width.

4.1. *Extinction*

Extinctions toward all three PNs are small. We do not estimate c owing to the limitations discussed in § 2. For NGC 6543, we adopt $\langle c \rangle = 0.2$—Middlemass, Clegg, & Walsh (1989, hereafter MCW); for NGC 6826, $\langle c \rangle = 0.17$—an intensity-weighted average from measurements by Ba88; for NGC 7009, $\langle c \rangle = 0.12$—Barker (1983, hereafter Ba83). c has its usual meaning. The values of Tables 1–3 were corrected for reddening using these values of $\langle c \rangle$ and the reddening curve for the general interstellar medium by Mathis (1990).

4.2. *Density*

The densities derived from $[S\ II]_{neb}$ and $[Cl\ III]_{neb}$ lines, $n(S^{+})$ and $n(Cl^{++})$, are shown in Table 4 for the important features discussed in this paper. These and the temperatures were obtained by solving the equation of statistical equilibrium for a five-level atom using collisional cross sections from Mendoza (1983), except that the collision strengths of [Ar IV] were taken from Zeippen, Butler, & Le Bourlot (1987) and those of [Cl III] were taken from Butler & Zeippen (1989).

The results for $n(S^{+})$ and $n(Cl^{++})$ are shown in Table 4, rounded to the nearest 10. Generally the two methods of mea-

TABLE 4

ELECTRON TEMPERATURES AND DENSITIES OF OBSERVED FEATURES

Nebula	NGC 6543			NGC 6826		NGC 7009		
Feature	N rim*	N cap*	N ansae*	SE rim	SE ansae*	W rim	W cap*	W ansae*
$n(S^+)$ cm^{-3}	4600	5000	2200	800 *600*	1000 *1400*	4900 *4000:*	4100 *3600*	1000
$n(Cl^{++})$ cm^{-3}	4680	5100	900:	370	-.-	1500:	9600	-.-
$T(N^+)$ °K	9300	9000	7400	7700	7600	10,000	9600 *9880*	8100
$T(O^{++})$ °K	8000	7900	8200	9400 *9100*	9200 *8900*	9400 *9600*	9600 *9400*	11,500
				final adopted values				
n cm^{-3}	4600	5000	2200	800	1000	4900	4100	1000
T °K	8700	8500	7800	8600	8400	9700	9600	see text

NOTE.—Numbers in italics are from Ba88 (NGC 6826) and Ba83 (NGC 7009).

suring the densities agree within the errors (about 10%) except where the [Cl III] lines are weak, or the lines are in the low-density limit. The one exception is the W FLIER of NGC 7009. For comparison, results obtained by Ba83 in very similar pointing positions (with a $\approx 3''$ aperture) are shown in italics in Table 4. The agreement with our results is excellent, and well within the mutual errors.

In NGC 6543 our line ratio [S II] λ6731/6717 is typically 1.8 in the bright, inner "core" of the nebula, close to the value of about 1.9 measured by Miranda & Solf (1992, hereafter MS). Strangely, we disagree with MS by a factor of 2 on the derived value of $n(S^+)$. On the other hand, our value of $n(Cl^{++})$ is quite close to the large-aperture, intensity-weighted average density of 6000 cm^{-3} found by MS. MCW measured the [O II] λ3729/3726 line ratio through a wide aperture and derived a density $n(O^+)$ of 5140 cm^{-3} with large uncertainties.

For NGC 6826 our derived densities are lower than the wide-aperture, intensity-weighted $n(O^+)$ result of 2000 cm^{-3} by MCW. Jacoby, Quigley, & Africano (1987, hereafter JQA) used ratios of very carefully calibrated narrow-band CCD images to measure the density distribution throughout NGC 6826. Imposing our slit on their Figure 3*b* shows excellent agreement in $n(S^+)$ except for one region which is nearly coincident with the small, bright SE flier. Their results show a sharp increase in the derived density to $\approx$2400 cm^{-3} at this position, whereas we see no comparable increase. Perhaps the registration of their images is slightly in error, producing rapid changes in line ratios where gradients in surface brightness are largest.

In spite of its complex variations in emission measure, the density distribution measured in the inner regions of NGC 7009 is remarkably uniform (Fig. 7). However, in this region $n(Cl^{++})$ is much smaller ($\approx$1500 cm^{-3}) than $n(S^+)$ ($\approx$4900 cm^{-3}). These discrepancies are not understood. Note that Czyzak & Aller (1979) measure a different ratio of [Cl III] λ5518/λ5538 than do we. In view of its stronger intensity we adopt $n(S^+)$ at all locations—a decision supported by the results of Ba88.

4.3. *Temperature*

The results are shown in Table 4. Formal errors are about 500 K except where the auroral lines are weak. We do not deem the differences between $T(N^+)$ and $T(O^{++})$ to be statistically significant except for the W ansa of NGC 7009. We have therefore adopted average values of the temperature in subsequent sections, as shown at the bottom of Table 4. For the W ansa of NGC 7009, we have adopted both measured temperatures, one each for the appropriate ionization states.

NGC 6543, $T(O^{++})$ is nearly constant at a value of 8000 K. MCW find roughly similar results for $T(O^{++})$ in their large-aperature measurements of NGC 6543, as do Czyzak et al. (1968) and Aller & Czyzak (1983).

Our results in NGC 6826 and 7009 are all in excellent agreement with Ba83 and Ba88, as Table 4 indicates. MCW measure an average value of $T(O^{++}) \approx$ 10,400 K in NGC 6826, a rather disparate result from ours in view of the formal errors. Differences in sampling are unlikely to account for the discrepancy. On the other hand, our results agree well those of JQA. The distribution of $T(O^{++})$ found by JQA along our slit rises from 9200 to 9800 K at the FLIERs, but the present data do not confirm the increase of $T(O^{++})$ that JQA find near the FLIERs.

4.4. *Abundances*

Abundances have been derived based on the data presented in Tables 1–3 (note the discussion of uncertainties in these data in § 2) and the analysis precepts of Barker (cf. Ba83 and Ba88). The densities and temperatures shown at the bottom of Table 4 were used in the analysis as appropriate. It must be noted that the method used to derive abundances assumes ionization equilibrium. This assumption is not locally valid where shocks heat and ionize gas.

Corrections for unseen stages of ionization, i_{cf}, are based on the methods of Ba83. Larger values of i_{cf} are the most uncertain, though absolute uncertainties are very difficult to assess. The results are summarized in Table 5. Our estimates of abundances are based on an intensity-weighted average, and for elements other than He and O, the uncertainties are generally dominated by errors in estimating i_{cf}.

4.4. *Helium*

The present He^+ abundances are based on bright emission lines other than He I λ7065. The He^+/H^+ abundances agree extemely well with earlier measurements of 0.11 in NGC 6543 by MCW and 0.094 by Ba88 in NGC 6826. For NGC 7009, the He^{++} zone is ionization bounded. The sum of He^+/H^+ and He^{++}/H^+ constant at about 0.11, compared to 0.117 found by Ba83. As noted in § 3, no evidence of He abundance variations with slit position is seen.

The He I λ7065/Hα line ratio yields results that are consistently a factor of 3 larger than all the other He I lines for every nebula and position. This includes the λ5876 line which shares

TABLE 5

INTENSITY-WEIGHTED IONIC AND TOTAL ABUNDANCES

Nebula		NGC 6543			NGC 6826		NGC 7009		
Species	line	N rim*	N cap*	N ansae*	SE rim	SE ansae*	W rim	W cap*	W ansae*
He^+/H^+	3819	0.100	0.093	0.085	0.064	0.120	0.070	0.095	-.-
	4026	0.111	0.090	0.059	0.093	0.078	0.081	0.097	0.161
	4471	0.116	0.106	0.099	0.099	0.092	0.095	0.106	0.094
	4922	0.108	0.103	0.126	0.101	0.070	0.082	0.086	-.-
	5876	0.124	0.110	0.104	0.097	0.099	0.098	0.104	0.110
	6678	0.126	0.117	0.120	0.097	0.099	0.103	0.107	0.119
	wt avg	0.121	0.109	0.105	0.097	0.095	0.096	0.104	0.116
He^{++}/H^+	4541	-.-	-.-	-.-	-.-	-.-	0.012	0.0053	-.-
	4026	-.-	-.-	-.-	-.-	-.-	0.011	0.0049	-.-
He/H		**0.121**	**0.109**	**0.105**	**0.097**	**0.095**	**0.107**	**0.109**	**0.116:**
$10^5 N^0/H^+$	5200	-.-	0.21	0.27	0.056	0.043	-.-	0.12	0.56
$10^5 N^+/H^+$	5755	0.85	4.98	5.63	0.16	1.90	0.28	1.99	12.0
	6584	0.71	4.25	6.75	0.22	2.54	0.26	1.97	12.2
$i_{cf}(N)$		17.8	6.18	8.54	30.6	6.92	70.5	16.5	7.91
10^4 N/H		**1.26**	**2.75**	**6.0**	**0.83**	**1.76**	**1.84**	**3.44**	**10.**
$10^4 O^0/H^+$	6300	0.0055	0.14	0.19	-.-	0.0058	0.0040	0.10	0.87
	6363	0.0012	0.15	0.21	-.-	0.0050	-.-	-.-	-.-
$10^4 O^+/H^+$	3727	0.24	0.84	0.73	0.16??	0.72	0.074	0.35	0.50
	7320	0.56	1.80	4.54	0.62??	3.11	0.24	0.80	1.4
	7330	0.29	1.27	2.15	0.29??	1.51	0.21	0.73	14
$10^4 O^{++}/H^+$	4363	2.86	3.21	6.63	6.27	6.00	4.18	5.26	2.58
	4959	4.03	4.31	5.49	4.58	4.23	4.63	5.16	2.57
$i_{cf}(O)$		1.00	1.00	1.00	1.00	1.00	1.11	1.05	1.00
10^4 O/H		**4.27**	**5.16**	**6.24**	**4.74**	**4.98**	**4.71**	**5.52**	**3.94**
$10^4 Ne^{++}/H^+$	3869	0.92	0.83	0.95	0.84	0.73	0.83	1.19	0.83
$i_{cf}(Ne)$		1.06	1.20	1.14	1.03	1.17	1.13	1.12	1.53
10^4 Ne/H		**0.98**	**1.00**	**1.1**	**0.86**	**0.85**	**0.94**	**1.33**	**1.3**
$10^6 Ar^{++}/H^+$	7135	2.57	3.02	3.91	1.44	1.79	1.31	2.18	1.81
	5192	-.-	-.-	-.-	-.-	-.-	0.86	-.-	-.-
$10^6 Ar^{3+}/H^+$	4740	0.26	0.10	0.19	0.16	0.083	0.63	0.42	0.26
$i_{cf}(Ar)$		-.-	-.-	-.-	1.01	1.05	1.04	1.15	2.28
10^6 Ar/H		**≥2.8**	**≥3.1**	**≥4**	**1.6**	**2.0**	**2.0**	**3.0**	**5**
$10^6 S^+/H^+$	6717	0.19	1.23	2.12	0.027	0.16	0.15	0.86	4.10
	6731	0.19	1.23	2.13	0.026	0.16	0.15	0.86	4.15
	4076	-.-	-.-	-.-	0.12	1.61	-.-	-.-	-.-
$10^6 S^{++}/H^+$	6312	4.73	8.41	17.:	2.19	3.22	3.83	5.77	3.22
$i_{cf}(S)$		1.84	1.34	1.47	2.19	1.39	2.88	1.80	1.44
10^6 S/H		**9**	**13**	**29:**	**4.9**	**4.7**	**11**	**12**	**11**
$10^6 Cl^{++}/H^+$	5518	0.091	0.23	0.10	0.047	0.11	0.12	0.17	-.-
	5538	0.17	0.11	0.12	0.072	0.068	0.039	0.045	-.-
10^6 Cl^{++}/H^+		**0.12**	**0.18**	**0.11**	**0.061**	**0.085**	**0.098**	**0.14**	**-.-**

* Qualifies as a FLIER.

the same principal quantum number of the initial state ($n = 3$), and exactly the same final state ($2\,^3P$), as the λ7065 line. We have no reason to suspect that the measurement errors exceed 15%. The reason for the large He I λ7065 fluxes is not understood. Observations of the He I 4.3 μm line ($3\,^3P \rightarrow 3\,^3S$) might help to clarify the collisional and radiative population rates of the upper level ($3\,^3S$) of the He I λ7065 transition.

4.6. *Nitrogen, Oxygen, etc.*

Errors in i_{cf} notwithstanding, large N/H abundance gradients are seen with slit position in NGC 6543 (factor of 5), NGC 6826 (factor of 2), and NGC 7009 (factor of 5). Details are discussed in § 5. The uncertainty in these results is probably a factor of 2. Even so, the results for the low-ionization features are signficant and provide an important clue to their origin. We find no other credible variations in other elemental abundances—including oxygen, for which most significant ionization states have been successfully observed.

5. DISCUSSION OF INDIVIDUAL NEBULAE

5.1. *NGC 6543*

Most recent distance estimates lie between 0.7 and 1.4 kpc (Acker et al. 1992). Cahn, Kaler, & Stanghellini (1993, hereafter CKS) estimate 0.98 kpc using a modified statistical Shklovsky method. The large surrounding halo has been investigated by MCW and Bryce et al. (1992b). The central star, an Of/WR, H-rich–type star (Méndez 1992), is losing mass prodigiously: Perinotto, Cerruti-Sola, & Lamers (1989, hereafter PCL) analyzed *IUE* and optical stellar data and find that $L_{rad}/L_\odot = 10^{3.75\pm0.5}$, $v_{wind} = 1900$ km s^{-1} and $\dot{M}_{wind} \approx 10^{-7.4}\ M_\odot$ yr^{-1}. The wind luminosity, $L_{wind} = 0.5\ \dot{M}_{wind}\ v^2_{wind}$, is only 12 $L_\odot$ (assuming spherical outflow), or 0.2% of the total stellar luminosity L_{rad}.

An exhaustive, detailed study of the internal kinematics of NGC 6543 by MS (and confirmed by BPI) shows that the portions of the ring, caps, and ansae sampled by our slit have

velocities of ± 24, ± 3, and ± 25–30 km s^{-1}, respectively. Although the details are as complex as the morphology of NGC 6543 itself (Fig. 1), MS find the overall pattern of motions to have some intriguing symmetries. They argue that (1) the caps (their components DD′) have true space velocities between 28 and 38 km s^{-1} (making them bona fide FLIERs like the ring and ansae) and (2) the motions of the ansae are in accord with the suggestion of high-speed (perhaps 250 km s^{-1}), highly collimated flows from a precessing binary system (Balick & Preston 1987). If so, then highly supersonic shocks should contribute to the heating and ionization of the gas at the many interfaces between the many components. This is addressed later.

As noted in § 3, an inspection of Figure 5 shows no large variations in temperature or density through the various caps and ansae where they intersect the slit. The ansae lie within a smooth, lower surface brightness halo of unknown pressure. As for the rims, there is a temperature increase of about 2000 K relative to their surroundings. The locally high temperature suggests that shock heating could be important locally. This is corroborated by the long-slit spectra of Walker & Aller (1970).

The caps and ansae show N/H abundance enhancements of factors of 2 and 5 respectively.

Kreysing et al. (1992) surveyed many PNs for evidence of extended soft X-ray emission. By far the brightest of the detected PNs is NGC 6543. Curiously, the soft X-rays are especially intense at (or very near) the caps. The existence of X-rays suggests that either the fast wind or a very hot medium forms an interface at the caps. If so, then the observed spectrum of the caps might be explained by some combination of X-ray ionization and/or heating in a largely neutral region as well as stong pressure gradients and shocks driven into largely neutral gas. Soft X-rays tend to produce a spectrum very rich in lines of all stages of ionization (see the summary by Netzer 1990) and may help to account for the large variety of low-ionization lines represented in the spectrum of the caps. Curiously, there is no trace of He II λ4686 or of highly ionized lines from iron in the nebular spectrum (note: X-ray emission also arises in BD +30°3639, a very low ionization PN with no He II λ4686 and only weak [O III] emission). Thus the local importance of X-ray ionization in the caps, or elsewhere in the nebula for that matter, is doubtful.

5.2. *NGC 6826*

Most recent distance estimates lie within 0.7 and 1.6 kpc (Acker et al. 1992). CKS estimate a distance of 1.6 kpc. The large surrounding halo has been investigated by MCW and Bryce, Meaburn, & Walsh (1992a). The central star has an O3f-type "H-rich" spectrum (Méndez 1992). PCL find $L_{\rm rad}/L_{\odot} = 10^{3.88\pm0.7}$, $v_{\rm wind} = 1750$ km s^{-1}, and $\dot{M}_{\rm wind} \approx 10^{-7.2} M_{\odot}$ yr^{-1}. $L_{\rm wind}/L_{\rm rad} \approx 0.2\%$ in NGC 6826.

The morphology of the entire nebula, which closely resembles NGC 3242 (Paper I), is the simplest of the PNs studied in the present paper. The ansae appear as an almost symmetric pair of outward-moving bow shocks on the major axis of the shell. There is marginal evidence of a kinematic "flare" in the line measurements in the ansae (BPI), as might be expected from shocked gas "splashing" at the stagnation point of a bow shock.

BPI find the shell of the nebula is expanding at a velocity of 15 or 20 km s^{-1}. The speeds of the ansae are much higher: ± 60 km s^{-1} after correction for inclination effects, easily qualifying them as FLIERs. The large velocities and bow-shock morphologies of the ansae suggest that a compressed, shocked gas layer should be present. In contrast, as suggested in Figure 6, the ansae have similar temperatures and densities as their surroundings. We shall discuss this further in § 6.

The N/H abundance of the ansae of NGC 6826 is twice that of the rim and the nebular shell.

5.3. *NGC 7009*

Most recent distance estimates lie between 0.7 and 1 kpc (Acker et al. 1992). CKS estimate 1.2 kpc. The spectral type of the nucleus is an H-rich O star (Méndez 1992). PCL find $L_{\rm rad}/L_{\odot} = 10^{4.02\pm0.3}$, $v_{\rm wind} = 2770$ km s^{-1}, and $\dot{M}_{\rm wind} \approx 10^{-8.6} M_{\odot}$ yr^{-1}. Consequently $L_{\rm wind} \approx 2\ L_{\odot}$, or 0.02% of $L_{\rm rad}$.

The internal kinematics were studied in detail by BPI in [N II] and by Reay & Atherton (1985, hereafter RA) in [O I]. The [N II] and [O I] kinematics are essentially identical. The caps and ansae have velocities of ± 24 and ± 6 km s^{-1}, respectively, with the sign of the velocity being different for adjacent pairs of caps and ansae. RA propose that after corrections for projection effects, and assuming purely radial motions, the caps have equal and opposite space motions of 38 km s^{-1} along one axis at an inclination of 51°, whereas the ansae have even higher velocities of 60 km s^{-1} on another axis of inclination of 84°. These calculated velocities are somewhat dependent on the adopted distance of 0.74 kpc; at 1.2 kpc the velocities would be larger. In any case, their results suggest that the features that we have designated as caps and ansae are actually *two* pairs of FLIERs on different axes for which RA determine ages 1100 and 1500 yr, respectively.

The caps and ansae of NGC 7009 resemble their counterparts in NGC 6543. Both sets of caps are thin axial filaments of low ionization and highly supersonic velocities, and both exhibit weak lines of Ca, Fe, and Si in their spectra. In both cases the caps (ansae) have N/H enhancements of factors of 2, (5). Essentially the same N/H over abundances were derived from noisier data by Czyzak & Aller (1979).

We are unable to determine whether soft X-ray emission has been observed near the caps of NGC 7009. A search for X-rays from NGC 7009 might prove to be interesting.

The ansae of NGC 7009 are of special interest because they are relatively bright FLIERs which can be studied virtually in isolation from a bright background of emission. The important spectroscopic results for the ansae are found in Figures 4 and 7. In many respects the ansae resemble the FLIERs found outside the shell of NGC 7662 (Paper I). Very interestingly, [O III]/Hβ, [N II]/Hα, [S II]/Hα, and [O I]/Hα are *all* enhanced relative to the nebular core (Table 3). Enhancements are largest for lines of relatively low ionization. The ansae appear to be very nitrogen-rich: N/H is more than 5 times the value observed in the rims.

The thermal and ram pressures of the ansae, relative to their (unobservably faint) immediate surroundings, are not known. But there is strong indirect evidence that their pressures are larger. Somewhat reminiscent of the FLIERs of NGC 3242 and 6826, the ansae of NGC 7009 resemble bow shocks with "hammerheads" at the leading edge, suggesting the existence of a significant upstream ram pressure into which the FLIERs are moving. There are interior columns of relatively bright gas along the symmetry axes which connect the caps and ansae (see Fig. 85 in Schwarz, Corradi, & Melnick 1992). Hence there seems to be evidence of a strong hydrodynamic interation between the ansae and the local gas. There may also be jets, much as those in NGC 7354 and 7662. Although our slit lies

close to these faint columns, the spectra are noisy in these regions. The emission line widths do not appear to flare at the heads of the bow shocks; however, much deeper echelle observations than those of BPI are needed to clarify this point.

6. DISCUSSION

It is useful to summarize the essential observable characteristics of FLIERs before proceeding: FLIERs are pairs of small ($\approx$0.01 pc) low-mass ansae, jets, knots, or strings of knots found on equal and opposite sides of the PN nucleus. Pairs always lie on or near a nebular symmetry axis. All known FLIERs have much higher velocity (always supersonic) and lower ionization than immediately adjacent gas, yet often the same temperature and density. Their N/H abundance ratios are much enhanced relative to the gas that envelops them, suggesting a recent stellar origin for the gas. Although their thermal pressures match those of their surroundings, FLIERs should interact hydrodynamically with their environment because their ram pressures are an order of magnitude larger than the confining pressure around them. Therefore, bow shocks are expected.

6.1. *FLIERs in Other PNs*

We next consider other PNs which might show similar types of structures. FLIERs embedded in NGC 3242 and 7662 were discussed in Paper I. They show virtually all of the same characteristics as those of the present study, except some are further from the PN's nucleus and lie far outside the shell.

Other authors have examined small, low-ionization features outside the bright shells of other PNs. Chu et al. (1991) found three features (H, H′, F) outside of NGC 6751 which appear to be FLIERs. Low-dispersion spectra show that [N II]/Hα is of order 2 in the FLIERs, much more extreme than the present sample of FLIERs. A mild radial increase in the N/O abundance in the FLIERs was noted. No discussion of the physical conditions specific to these regions is given.

López, Roth, & Tapia (1993) have studied the elliptical PN Fg 1. Two symmetrically bent strings of knots which extend outward from the outer edge of the nebular shell are "highly reminiscent of H-H objects." Measured radial velocities (+26, −17 km s^{-1}) qualify the knots as FLIERs. The [N II]/Hα ratios in the innermost, brightest knots at the base of the jets are 2.7 and 1.9, respectively. They report: "In the knots the [radiative] conditions are either very low or [ionization is] by collisional mechanisms." Abundances in the knots were not determined.

Another elliptical PN, NGC 6905, has been known to have a pair of low-ionization knots lying outside the nebular core (e.g., Balick 1987). These were studied by Cuesta, Phillips, & Mampaso (1993) who show the knots to be bone fide FLIERs at velocities of about $\pm$40 km s^{-1} before correction for projection effects. The [N II]/Hα ratios are 1 and 2 in the two FLIERs. Cuesta et al. argue that the FLIERs are produced by converging flows of shocked gas. (Note: they implicitly presume that the FLIERs are shielded from stellar untraviolet heating and ionization.)

Several bipolar nebulae have been studied by Corradi & Schwarz (e.g., 1993a, b). Many of these PNs also show knots and jets along their symmetry axes. Knot velocities range up to $\pm$200 km s^{-1}. Phenomenologically these knots are FLIERs; however, their association with bipolar PNs suggests that their formation process(es) might be unrelated to that of FLIERs in elliptical PNs. In any event, no spectrophotometric measurements of the FLIERs in bipolar PNs are yet available, so we do not consider the FLIERs of bipolar PNs further in this paper.

6.2. *Paradigms*

We turn now from a description of FLIERs to an effort to interpret the results. We consider possible better studied analogies to determine whether and to what extent they might serve as interpretive paradigms for the observations of FLIERs.

Low-ionizations H-H objects share many of the same properites as FLIERs. Both are small in at least one dimension; both have very strong emission lines of O°, S^+, N^+, etc.; both have small masses and large velocities, and the spatial distributions of both all point to an origin somehow associated with a central star system that has ejected collimated material along a preferred axis. Taking this analogy to H-H objects further, FLIERs could be recent ejecta which is collimated by some complex mechanism such as mass-transfer binary or accretion disk systems (Morris 1987; Soker 1990; Soker & Harpaz 1992; Livio 1993). By the time they can be recognized at FLIERs, the ejected material appears as a knot or jet propagating through a smoother, probably older medium. In this case bow shocks should arise, and indirect evidence for shock excitation in some PNs has been suggested by Peimbert, Sarmiento, & Fierro (1991) and Trammel, Dinerstein, & Goodrich (1993).

Of course important differences between FLIERs and H-H objects exist as well, e.g. chemical abundances of H-H objects are generally solar, and there is no hot star to provide heating and ionization by ultraviolet photons. But these differences are almost certainly the result of conditions unique to PNs and not necessarily relevant to the issue of FLIER morphology, size, and motion. Consequently it may be revealing to inquire: to what extent is the low-ionization, bow-shock H-H analog consistent with the details of the observations?

Consider first the emission-line ratios. The spectral properties of bow shocks have been studied in the context of H-H objects by Hartigan, Raymond, & Hartmann (1987, hereafter HRH), Hartigan (1989), and Noriega-Crespo, Böhm, & Raga (1989) and Böhm, Noriega-Crespo, & Solf (1993). Their quantitative predictions are extremely sensitive to assumptions about geometry (bow or planar shocks), chemical abundances, magnetic fields, and shock velocities. Small differences in initial conditions often produce large variations in predicted line ratios. A detailed comparison between the line ratios of FLIERs and H-H objects requires better observational data for the FLIERs.

Nonetheless, one might ask for minimal consistency under *any* reasonable assumptions. For example, HRH produce tables of predictions of bow shocks in H-H objects for near-solar abundances and under a wide range of assumed conditions. No model computed by HRH for which the shock speed v_S is in accord with the velocities of FLIERs, $v_S \leq 100$ km s^{-1} accounts for [N II]/H$\alpha > 0.5$. On the other hand, values of [O I]/Hα between 0.01 and 2 are possible at these velocities. The large N/H abundance ratios that we have found for FLIERs—about 5 times greater than the value adopted by HRH—easily explains these discrepancies.

On minor problem with *pure* shock models is that line intensity ratios in the literature do not consider the ionization and heating of FLIERs by ultraviolet photons from a nearby star. We can anticipate that the calculated values of the [N II]/Hα and [O I]/Hα ratios will be far smaller (for solar abundances) than indicated by HRH when stellar preionization (which

tends to truncate the line-emitting recombination zone behind the shock) is added to the shock model computations.

Much more of a problem for shock models is the observed ionization stratification seen in Figure 4. Gas at the leading (outward-facing) edge of any shock is more highly ionized than in the recombination zone downstream (where [N II] and [O I] lines preferentially arise). For bow shocks, the region of highest ionization is at the tip of the cone (e.g., HRH Noriega-Crespo et al. 1989, and Böhm et al. 1993). In planar shocks the region of highest ionization is also on the upstream side of the shock. However, the observed pattern of ionization (Fig. 4) shows the reverse behavior!

6.3. *Photon Excitation*

Their low ionizations, that is, their high [O I]/Hα, [S II]/Hα, and [N II]/Hα ratios, are among the most prominent characteristics of FLIERs. Generally speaking, standard photoionization models fail to produce these observed ratios to an order of magnitude unless FLIERs are affiliated with regions of partial ionization, such as those associated with nonequilibrium ionization fronts (I.F.'s). Also, Lame & Ferland (1991) and Richer, McCall, & Martin (1991) have shown that very hard photons (with large mean free paths) emitted by extremely hot central stars ($> 10^5$ K) can create large volumes of partially ionized gas. The resulting line ratios can be close to those that we observe for FLIERs.

The latter idea can be quickly disposed. For one thing, the central stars of the PNs studied here lie between 40 and 75,000 K, too cool to produce large volumes of partially ionized gas. For another, FLIERs are much too small in size to fit this picture of extended, partially ionized regions.

I.F.'s hold more promise. The small sizes of FLIERs, ≈ 0.02 pc, are consistent with the formation of an I.F. in a medium of density 3000 cm^{-3} located about 0.1 pc from a cooler nucleus emitting 10^{47} ionizing photons s^{-1}. Also, the radial gradients in fractional ionization (e.g., O° arising at larger radius than N^+ or O^+) seen in Figure 4 are naturally explained.

Despite the success of I.F.'s in explaining the line ratios and the ionization gradients, a wide range of problems plagues this type of explanation. Very clearly, photoionization models are impotent to account for many characteristics of FLIERs, including their small sizes, high nitrogen abundances, their pairwise distributions, or their high velocities. For example, the possbility of photon acceleration of FLIERs can safely be discarded owing to the low efficiency (1%) with which radiation pressure is converted into bulk gas kinetic energy (Dyson & Williams 1980). Even the idea that a FLIER can be affiliated with an I.F. is suspect, especially since many PNs with FLIERs have large and highly ionized outer halos containing half of their mass (MNW).

6.4. *Instabilities*

Are FLIERs the result of instabilities at the leading edges of shells which evolve to become opaque to ionizing radiation (Kahn & Breitschwerdt 1990; Breitschwerdt & Kahn 1990)? The instability hypothesis accounts nicely for the small sizes, locations, and low ionizations of FLIERs, but little else. Why are such regions located almost universally along the PN symmetry axis? What accounts for the large velocities of FLIERs? Why is the nitrogen abundance high only in the instabilities? While instabilities may play some sort of role in the early evolution of FLIERs, they do not provide a very complete explanation.

6.5. *Shadows*

Can FLIERs be ionization shadows where gas is not illuminated by direct stellar photons? (Such shadows are cast behind dense knots seen in NGC 6853 and 7293.) Diffuse emission is consistent with the lower ionization, yet similar density and temperature, of FLIERs relative to the surrounding gas. Nonetheless, there are several problems. First, the velocities and pairing of FLIERs are not naturally explained. Second, the recombination times in shadows are shorter than the dynamical lifetimes of FLIERs, meaning that the low-ionization gas could not have been ionized previously. Hence shadows seem unlikely.

Other analogs to FLIERs are much more difficult to find. Jets associated with SS 433 have much higher velocities and rather different morphologies than FLIERs, and the physics that describes their interaction with an upstream fluid is largely different. There are small low-ionization knots seen in some H II regions, but these are generally believed to be H-H–like objects.

In summary, no simple classical picture, such as bow shocks or I.F.'s, incorporates a significant fraction of the observations of FLIERs into any sort of a coherent framework.

7. CONCLUSIONS

The nature of FLIERs is not yet clear. Their highly supersonic velocities and large N/H abundance ratios suggest that FLIERs have been recently expelled from the PN nucleus and move with velocities at which shocks (probably bow shocks) should play a central role in heating, cooling, and formation of the local emergent spectrum. However, several observations, especially the radially decreasing fractional ionization, are in conflict with this expectation.

In Paper I we reviewed arguments that FLIERs are generated by the star and not produced by an in situ process, such as hydrodynamic focusing of flows, followed by some sort of instability that generates observable knots or jets of emitting gas. Since that paper was written, new and more detailed radiation gas dynamic models of evolving PNs have been generated by Frank (1993) and Mellema (1993). They find that relatively dense knots often form along the symmetry axis shortly after the onset of the fast wind from the nucleus. The dense knots are situated near the leading edge of the expanding hot bubble, but not generally where FLIERs are situated.

Whether these knots are FLIERs is dubious. The models, which include radiative cooling, predict that the knots are considerably hotter than the observed temperatures of 10^4 K and have lower velocities (≤ 30 km s^{-1}) than FLIERs. The knots are formed from material in the shell, meaning that no enhancement of nitrogen in expected.

7.1. *Future Research*

From an interpretive standpoint, models of shocks moving through a highly ionized H II region are urgently needed. For example, it is by no means obvious that classical shocks in a highly photoionized region will produce the strong enhancements of low-ionization lines that are seen in FLIERs. The degree of shock compression in such a medium also needs quantitative analysis.

Also, the idea of a mechanism to eject N-enriched material from the nucleus needs to be evaluated from a theoretical standpoint. Livio (1993) has just begun to explore the physics of mass transfer systems, and it is not yet clear whether highly

processed material from the compact nucleus in a mass-transfer system is feasible.

On the observational side, imaging of the isolated ansae using very narrow band filters and at very high spatial resolution may yet reveal the outlines of bow shocks in embedded FLIERs, such as those in NGC 3242 and 6826, or isolated FLIERs, such as those in NGC 7009 and 7662. At the very least, searches for and maps of neutral atomic or molecular gas in FLIERs, if successful, would clearly provide important insight into their nature and origin.

Curiously, the kinematic ages of FLIERs appear to be smaller than the ages of the nebular shells in which they are situated. This means that if FLIERs are neutral knots, they are ejected that way while the star is relatively hot—certainly after the AGB evolution that produces the surrounding shell. Conceivably the H_2 knots now seen along the major axis of NGC 7027 outside the ionized part of the shell (Graham et al. 1993) could develop into FLIERs once the ionization front engulfs them. If so, the velocities of the H_2 knots should be measured to test this idea—a prediction of about 50 km s^{-1} seems like a reasonable expectation.

Also, it is important to search PNs in earlier phases of their development in order to find evidence of any precursor to FLIERs. More careful studies of the knots found in the Frosty Leo nebula (Morris & Reipurth 1990) might yield interesting and relevant results. Other elliptical and bipolar proto–planetary nebulae should also be studied.

The FLIER-like features associated with NGC 6751, Fg 1, and other PNs need more careful scrutiny to see if their properties connect them to the FLIERs studied in this paper. It seems reasonable to expect that they may be FLIERs in a later stage of their development.

In summary, FLIERs are a class of very unusual nebular features. They resemble H-H objects in many ways, such as their small sizes, space velocities, and low ionizations, but are clearly very different in others, such as anomalous enhancements of nitrogen. All the available evidence points to a recent stellar origin, though it is by no means clear how a star can produce them at a late stage of its mass loss. Perhaps FLIERs result from a complex interaction between a contact binary, but the feasibility of such a process is speculative at this time.

It is a pleasure to thank the staff of Palomar Observatory for their hospitality and J. Chengalur for this generous help with the observations. John Raymond proffered valuable interpretive insight, and L. Stanghellini enthusiastically provided stellar data. We acknowledge the very important compilation of emission lines from the literature by J. Kaler and L. Browning. We thank these authors for their willingness to allow us to use the catalogue prior to publication. B. B. is grateful for support by grants from the National Science Foundation (AST 89-13639), the University of Florence, and the National Research Council of Italy. The kind hospitality of Osservatorio Astrofisico di Arcetri was particularly pleasant if not frequently deliciously distracting. Y. T. and A. H. were supported in part by the National Astronomy and Ionosphere Center which is operated by Cornell University under a cooperative management agreement with the National Science Foundation. Observations at Palomar Observatory were made as part of a continuing collaborative agreement between the California Institute of Technology and Cornell University.

REFERENCES

Acker, A., Ochsenbein, F., Stendholm, B., Tylenda, R., Marcout, J., & Schohn, C. 1992, Strasbourg-ESO Catalogue of Galactic Planetary Nebulae (Garching: ESO)
Aller, L. H. 1941, ApJ, 93, 236
———. 1984, Physics of Thermal Gaseous Nebulae (Dordrecht: Reidel)
Aller, L. H., & Czyzak, S. J., 1983, ApJS, 51, 211
Aller, L. H., & Keyes, C. D. 1988, Proc. Natl. Acad. Sci., 85, 2417
Balick, B. 1987, AJ, 94, 671
Balick, B., & Preston, H. L. 1987, AJ, 94, 958
Balick, B. Preston, H. L., & Icke V. 1987, AJ, 94, 1641 (BPI)
Balick, B., Rugers, M., Terzian, Y., & Chengalur, J. N. 1993, ApJ, 411, 778 (Paper I)
Barker, T. 1983, ApJ, 267, 630 (Ba83)
———. 1988, ApJ, 326, 164 (Ba88)
Böhm, K. H., Noriega-Crespo, A., & Solf, J. 1993, ApJ, 416, 647
Breitschwerdt, D., & Kahn. F. D. 1990, MNRAS, 244, 521
Bryce, M., Meaburn, J., & Walsh, J. R. 1992, MNRAS, 259, 629
Bryce, M., Meaburn, J., Walsh, J. R., & Clegg, R. E. S. 1992, MNRAS, 254, 477
Butler, K., & Zeippen, C. J. 1989, A&A, 208, 337
Cahn, J. H., Kaler, J. B., & Stranghellini, L. 1992, A&AS, 94, 399
Chu, Y.-H., Manchado, A., Jacoby, G. H., & Kwitter, K. B. 1991, ApJ, 376, 150
Corradi, R. L. M. & Schwarz, H. E. 1993a, A&A, 268, 714
———. 1993b, A&A, 269, 462
Cuesta, L., Phillips, J. P., & Mampaso, A. 1993, A&A, 267, 199
Czyzak, S. J., & Aller, L. H., 1979, MNRAS, 188, 229
Czyzak, S. J., Aller, L. H., & Kaler, J. B. 1968, ApJ, 154, 543
Dyson, J. E. & Williams, D. A. 1980, Physics of the Insterstellar Medium (New York: Wiley), 143–145
Frank, A. 1993, Ph.D. thesis, Univ. of Washington
Graham, J. R., Serabyn, E., Herbst, T. M., Mathews, K., Neugebauer, G., Soifer, B. T., Wilson, T. D., & Beckwith, S. 1993, AJ, 105, 250
Hartigan, P. 1989, ApJ, 339, 987
Hartigan, P., Raymond, J., & Hartmann, L. 1987, ApJ, 316, 323 (HRH)
Jacoby, G. H., Quigley, R. J., & Africano, J. L. 1978, PASP, 99, 672 (JQA)
Kahn, F. D., & Breitschwerdt, D. 1990, MNRAS, 242, 505
Kreysing, H. C., Diesch, C., Zweigle, J., Staubert, R., Grewing, M., & Hasinger, G. 1992, A&A, 264, 623
Lame, N. J., & Ferland, G. J. 1987, ApJ, 367, 208
Livio, M. 1993, in The Theory of Accretion Disks II (ESO: Garching), in press
López, J. A., Roth, M., & Tapia, M. 1993, A&A, 267, 194
Mathis, J. S. 1990, ARA&A, 28, 37.
Mellema, G. 1993, Ph.D. thesis, Leiden Univ.
Méndez, R. H. 1992, in IAU Symp. 145, Evolution of Stars: The Photospheric Abundance Connection, ed. G. Michaud & A. Tutukov (Dordrecht: Kluwer), 378
Meudoza, C. 1983, in IAU Symp. 103, Planetary Nebulae, ed. D. R. Flower (Dordrecht: Reidel), 143
Middlemass, D., Clegg, R. E. S., & Walsh, J. R. 1989, MNRAS, 239, 1 (MCW)
Miranda, L. F., & Solf, J. 1992, A&A, 260, 397 (MS)
Morris, M. 1987, PASP, 99, 1115
Morris, M., & Reipurth, B. 1990, PASP, 102, 446
Netzer, H. 1990, in Active Galactic Nuclei, ed. T. J.-L. Courvoisier-Thierry & M. Mayor (Berlin: Springer-Verlag), 57
Noriega-Crespo, A., Böhm, K. H., & Raga, A. C. 1989, AJ, 98, 1388
Osterbrock, D. E. 1990, Astrophysics of Gaseous Nebulae and Active Galactic Nuclei (Mill Valley CA: University Science Books)
Peimbert, M., Sarmiento, A., & Fierro, J. 1991, PASP, 103, 815
Perinotto, M., Ceruti-Sola, M., & Lamers, H. J. G. L. M. 1989, ApJ, 337, 382 (PCL)
Reay, N. K., & Atherton, P. D. 1985, MNRAS, 215, 233 (RA)
Richer, M. G., McCall, M. L., & Martin, P. G. 1991, ApJ, 377, 210
Schwarz, H. E., Corradi, R., & Melnick, J. 1992, A&AS, 96, 23
Soker, N. 1990, AJ, 99, 1869
Soker, N., & Harpaz, A. 1992, PASP, 104, 923
Solf, J., Böhm, K. H., & Raga, A. 1988, ApJ, 334, 229
Trammell, S. R., Dinerstein, H. L., & Goodrich, R. W. 1993, ApJ, 402, 249
Walker, M. F., & Aller, L. H. 1970, ApJ, 161, 917
Zeippen, C. J., Butler, K., & Le Bourlot, J. 1987, A&A, 188, 251